Acta Oceanol. Sin., 2019, Vol. 38, No. 4, P. 167–174
https://doi.org/10.1007/s13131-019-1420-8
http://www.hyxb.org.cn
E-mail: hyxbe@263.net

Analysis of temperature inversion in the Zhujiang River Estuary in July 2015

Xirong Chen[1], Zhenyu Sun[1], Hongyang Lin[1], Jia Zhu[1]*, Jianyu Hu[1]

[1] State Key Laboratory of Marine Environmental Science, College of Ocean and Earth Sciences, Xiamen University, Xiamen 361102, China

Received 13 June 2018; accepted 10 October 2018

Abstract

This study investigates the temperature inversion phenomenon in the Zhujiang (Pearl) River Estuary (ZRE) using hydrological data collected in a summer cruise during July 6–17, 2015. The results suggest that temperature inversion occurred primarily near the salinity front, with an average temperature difference (ΔT) of 0.42°C between the inversion layer and the underlying water. The inversion layer was approximately 4 m thick on average, with an upper boundary at a depth of 1–6 m and a lower boundary at a depth of 3–10 m. Different mechanisms and dynamic processes were responsible for temperature inversion in different parts of the study area. (1) At the salinity front in the west of the ZRE, the measurements collected by CTD (conductivity, temperature, and depth) showed that the low-salinity water mass on the inner side of the front was approximately 2°C cooler than the high-salinity water mass on the outer side. Temperature inversion occurred when the cooler low-salinity water overlapped the warmer high-salinity water near the front due to the driving force of the background flow. (2) Inversion layers occurred at the mouth of the Taiping waterway as a result of varying horizontal flow between two different water masses under the effects of tides and runoff. (3) To the southwest of Hong Kong, temperature inversion occurred due to the interaction of upwelling and the salinity front.

Key words: Zhujiang (Pearl) River Estuary, temperature inversion, summer

Citation: Chen Xirong, Sun Zhenyu, Lin Hongyang, Zhu Jia, Hu Jianyu. 2019. Analysis of temperature inversion in the Zhujiang River Estuary in July 2015. Acta Oceanologica Sinica, 38(4): 167–174, doi: 10.1007/s13131-019-1420-8

1 Introduction

The decrease in sea water temperature with increasing depth is a well-known feature in low- to mid-latitude open oceans. However, oceanic temperature inversion, where temperature increases with depth, has also been widely documented and has been recorded by observational data for the Arabian Sea, the Bay of Bengal, the sub-polar waters of the North Pacific, and the offshore waters of the China seas (Thadathil et al., 2002; Ueno and Yasud, 2005). Temperature inversion forms by way of two main mechanisms (Thadathil and Gosh, 1992; Chen et al., 2006; Nisha et al., 2009): (1) The precipitation cooling mechanism, where sea surface cooling (induced by cold air, typhoons, or other extreme weather events) and local precipitation lead to the presence of low-temperature and low-salinity water at the surface, and (2) the advection mechanism, where low-temperature and low-salinity water is horizontally advected to superpose high-temperature and high-salinity water. Differences in the distribution of temperature reversal allow inversion phenomena in the East China Sea to be divided into five types (Lan et al., 1993): single reversal, double reversal, reversal type with intermediate cold water, reversal with intermediate warm water, and mixed reversal. This paper will follow this schema for the characterization of temperature inversions in its study area.

Temperature inversion can have an important impact on local oceanic conditions as well as on air-sea interactions. For example, it can affect vertical heat transfer and hence significantly influence the heat budget within the upper mixed layer (Han et al., 2001; Akhil et al., 2014). Temperature inversions are often associated with a low-salinity sea surface, which prohibits vertical mixing and thus reduces surface-subsurface exchange (Girishkumar et al., 2013). Temperature inversion has also been demonstrated to be a key factor in generating seasonal and interannual variability in sea surface temperature (SST) (Nagura et al., 2015).

Temperature inversion phenomena in the China seas are mainly found on the shelf of the East China Sea, with different types of temperature reversal observed throughout the year (Nagata, 1967; Yan, 1991; Yuan et al., 2010; Hou et al., 2010). In the Taiwan Strait, temperature inversion has particularly been observed during the northeasterly monsoon period (Qiu et al., 2012), when the precipitation cooling mechanism is found to be the main mechanism. However, temperature reversal phenomena have not previously been reported in the Zhujiang (Pearl) River Estuary (ZRE).

The circulation around the ZRE and its responses to tides, winds and buoyancy discharge during summer have been investigated numerically (Wong et al., 2003a, b ; Dong et al., 2004; Zu et al., 2014; Zu and Gan, 2015). Fresher water exiting from the estuary forms a buoyant plume over the shelf. This spreads eastward or southeast-ward in response to the southwesterly monsoon during summer (Ou et al., 2007). The winds of the East Asia summer monsoon also cause upwelling along the coast of the ZRE and a northeastward along-shore current. This coastal current

Foundation item: The National Basic Research Program of China under contract No. 2015CB954004; the National Natural Science Foundation of China under contract Nos 41776027, 41606009 and U1405233.
*Corresponding author, E-mail: zhujia@xmu.edu.cn

closely interacts with estuarine circulation in the ZRE (Dong et al., 2004). Besides wind forcing and buoyancy from river discharge, circulation in the ZRE is also forced by tides in summer. Tides are mainly semi-diurnal (M_2) and diurnal (K_1) around the ZRE and have a magnitude of approximately 1.0 m inside the ZRE. They are amplified and modulated as they propagate back and forth within the spatially variable water depth of the ZRE. Tides form a counterclockwise residual circulation (Mao et al., 2004).

During a summer cruise in 2015, we observed the presence of temperature reversal in several zones of the ZRE. This paper presents a detailed characterization of their features and a preliminary analysis of their formation mechanisms.

2 Data and methods

The 2015 summer cruise was conducted aboard the R/V *Kediao No. 8* during the period of July 6–17. The first leg of the cruise spanned July 6–12, visiting 50 observation stations (Fig. 1) and conducting 68 CTD (conductivity-temperature-depth) casts. The second leg spanned July 13–17, visiting 52 stations (Fig. 2) and making 60 CTD casts. The CTD used in the cruise was the Sea-Bird SBE 25, which has a temperature sensor accuracy of 0.001°C, a resolution of 0.000 2°C, a pressure sensor accuracy of 10 kPa, and a resoluttion of 0.68 kPa. The research vessel was also equipped with an RTI shipboard ADCP (600 kHz) and Thermosalinograph SBE 21. During the cruise, a fixed-point buoy was deployed near Sta. 2A14 (Fig. 2) to obtain the local daily averaged sea surface air temperature and SST, as shown in Fig. 3.

During the cruise, Typhoon Linfa landed on the coast at Lufeng City, Guangdong Province (22.656°N, 116.271°E) at approximately 12:00 (local time) on July 9 with a wind speed of 35 m/s. It then weakened to become a severe tropical storm and passed across the Zhujiang River (22.6°N, 113.7°E) with a wind speed of 15 m/s. Shortly afterwards, it gradually weakened and disappeared. The track of its low-pressure center in the region of the ZRE is shown by the cyan line in Fig. 1.

Taking the vertical distributions of seawater temperature and salinity at Sta. F302 as an example (Fig. 4), we describe the method by which the characteristic parameters of inversion layers were calculated. The change in temperature is calculated as follows: $\Delta T=T_L-T_U$ (Ueno and Yasud, 2005), where T_L is the maximum temperature in the inversion layer, with depth D_L being the lower bound of the inversion layer, and T_U is the minimum temperature in the inversion layer, with depth D_U being the upper bound of the inversion layer. A temperature inversion layer is regarded to exist if $\Delta T>0.1$°C. Stations at which the CTD data indicated the presence of an inversion layer meeting this requirement are shown as red dots in Figs 1 and 2; while their specific parameters are listed in Table 1.

3 Characteristics of temperature inversions detected

The stations at which a temperature inversion layer was de-

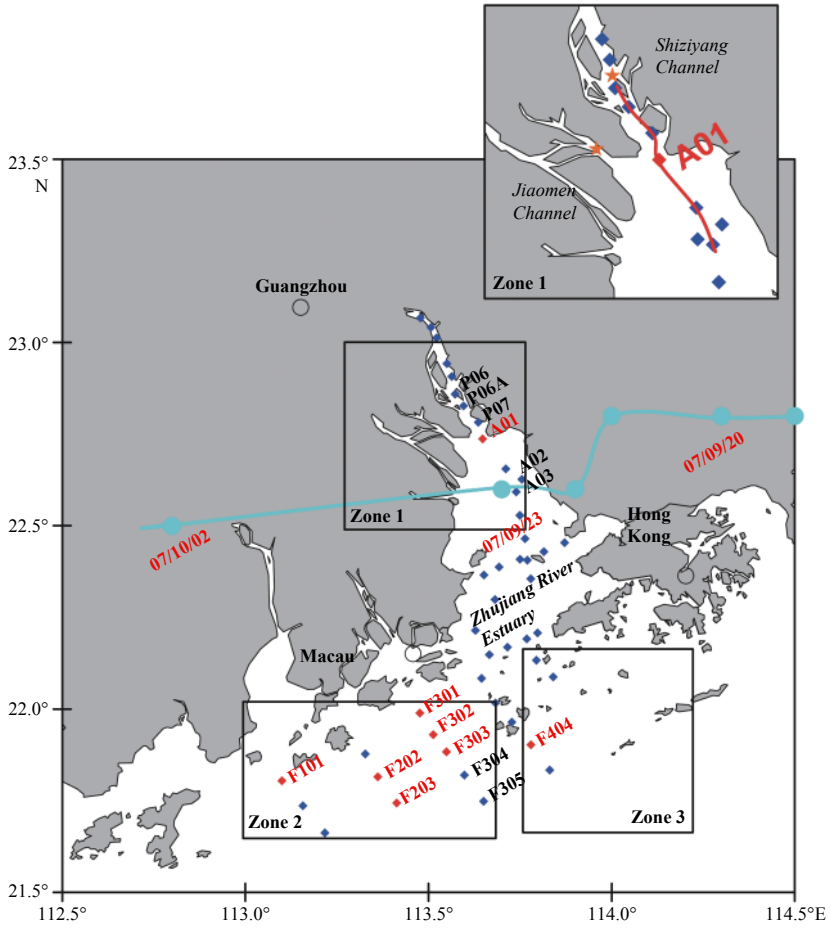

Fig. 1. Survey stations during the first leg of the cruise. Blue points represent CTD stations where no temperature inversion layer was detected; red points CTD stations where a temperature inversion layer was detected; and cyan line and dots track of Typhoon Linfa and the low pressure center of the typhoon, with dates and times marked in red (e.g., 07/10/02 means 02:00, July 10, 2015).

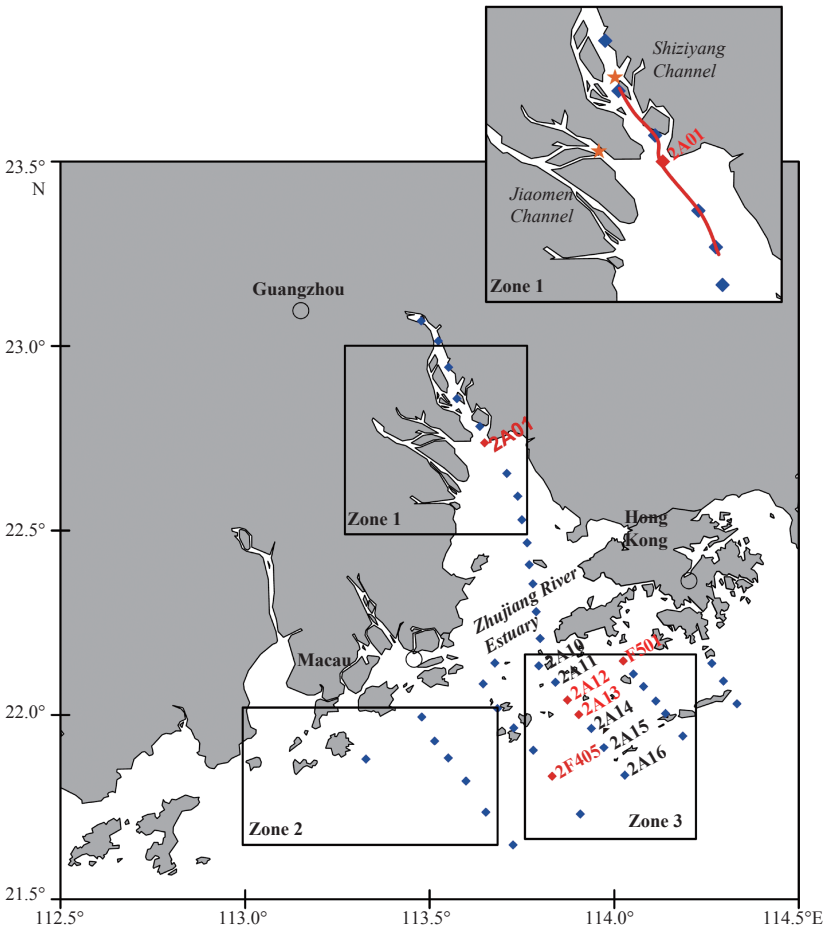

Fig. 2. Survey stations during the second leg of the cruise. Blue points represent CTD stations where no temperature inversion layer was detected; and red points CTD stations where a temperature inversion layer was detected. The black triangle near Sta. 2A14 is the location of a fixed-point buoy.

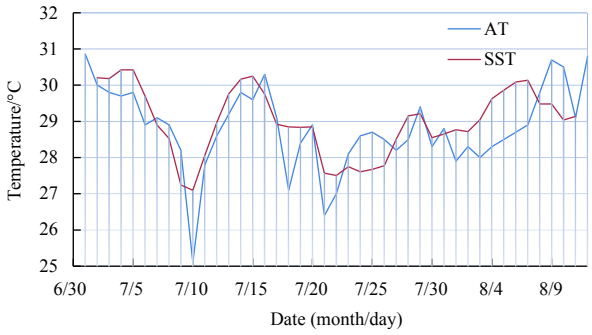

Fig. 3. Time variations of mean air temperature (AT) and sea surface temperature (SST) at buoy Sta. 2A14 in 2015.

tected are shown in Figs 1 and 2. Overall, temperature inversion was observed in three main zones: Zone 1 is at the confluence of the Shiziyang Channel, the Taiping Channel, and the Jiaomen Channel, Zone 2 is to the west of the ZRE, and Zone 3 is in the southwest of Hong Kong. The temperature difference in the inversion layers ranged from 0.11°C to 1.14°C, with an average value of 0.42°C, the upper bound was between 1 m and 6 m, the lower bound was between 3 m and 10 m, and the average thickness of the inversion layer was approximately 4 m. The characteristics of the inversion differed from one zone to another. Due to the effects of Typhoon Linfa, the daily mean sea surface air temperature and SST at the fixed-point buoy were extremely low on July 10, namely 25.00°C and 27.10°C, respectively.

The results in Table 1, Figs 1 and 2 show a temperature inversion layer in Zone 1 at Stas A01 and 2A01, where the water depth is about 14 m. The observations were made at 14:00 on July 10 and 16:00 on July 13, respectively and the observed temperature differences were 0.27°C and 0.47°C, respectively. A lower boundary was detected at 5 m. The vertical temperature and salinity distributions (Figs 5a, b) indicate that there was only one inversion layer and that its upper boundary was at the surface. A similar inversion layer was detected at both stations despite the water temperature at Sta. 2A01 being approximately 1°C higher than that at Sta. A01. Since 2A01 is proximate to A01 and both of their salinity profiles show low salinity values (0–10) and no obvious stratification, the mechanism of temperature inversion at 2A01 may be similar to that at A01.

Table 1 and Fig. 1 show the existence of another inversion layers at Stas F101, F203, F202, F301, F302, F303 and F404 in Zone 2, while Table 1 and Fig. 2 show the presence of an inversion layer at Stas 2F405, 2A12, 2A13 and 2F501 in Zone 3. The vertical distributions of temperature and salinity at representative stations (F302 and F303, 2F501 and 2A13) are shown in Fig. 5. The water in Zone 2 or Zone 3 can be divided into three different layers on the basis of vertical salinity gradient. The vertical salinity gradient is about 0.5 to 1.5 m^{-1} in the surface layer (spanning 0–5 m

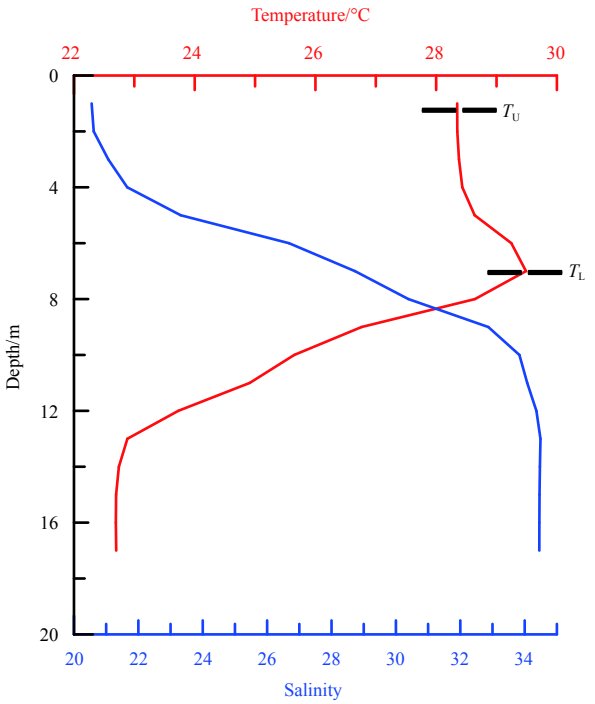

Fig. 4. Vertical distribution of temperature and salinity. T_L is the maximum temperature in the inversion layer; T_U is the minimum temperature in the inversion layer; $\Delta T=(T_L-T_U)>0.1$°C; the temperature profile is regarded as a temperature inversion layer.

depth) in Zone 2 and Zone 3, respectively. But their features become the opposite in the intermediate layer. The vertical salinity gradient is about 1.5 m^{-1} in the intermediate layer (~5–10 m) in Zone 2, while the vertical salinity gradient decreases to 0.5 m^{-1} in the intermediate layer (~5–15 m) in Zone 3. The salinity becomes essentially constant with depth below 10 m in Zone 2 and below 15 m in Zone 3. Therefore, the slightly different definitions of three layers in Zone 2 and Zone 3 are determined by their local characteristics of salinity profiles.

The corresponding temperature reversal phenomenon has following characteristics: (1) In Zone 2, the temperature difference of the inversion ranges from 0.11°C to 1.14°C, mainly falling into the surface layer where maximum vertical salinity gradient occurs, with the lower bound of the inversion layer between 4 m and 7 m, and the upper bound at 1 m. Among these inversion layers, the temperature reversal phenomena at Stas F301, F302 and F303 are most evident. The temperature inversions in all three stations are larger than 0.5°C, with the maximum value, 1.14°C, recorded at Sta. F302. Temperature inversion in this area was mainly observed during the first leg of the cruise. (2) In Zone 3, the coverage of fresh water in this zone was about 5 m during the second leg of the cruise, which led to the difference in the vertical distribution of salinity versus the other two zones. The temperature first decreases with increasing depth in the surface layer, and then there is a significant reversal in the intermediate layer where maximum vertical salinity gradient occurs in Zone 3. The upper bound of the temperature inversion layer is at 5–6 m, generally at the upper boundary of the intermediate water, while the lower bound is at 8–9 m; the reversal temperature difference ranges from 0.25°C to 0.54°C. (3) Generally, temperature inversion was mainly observed with the maximum vertical salinity gradient in either Zone 2 or Zone 3.

4 Dynamic mechanisms

As detailed above, temperature inversion layers were detected in three zones of the ZRE in July 2015. The dynamic mechanism by which these formed in each zone is investigated below. In addition, the principal dynamic mechanism for the formation of temperature inversions in the ZRE is the advection of ambient flows, in contrast with the findings of Qiu et al. (2012) in the Taiwan Strait.

The inversion phenomenon in Zone 1 was only observed at

Table 1. Characteristics of temperature inversions detected in the ZRE

CTD station	Date (month/day/year)	T_L/°C	D_L/m	T_U/°C	D_U/m	ΔT/°C
F101_01	07/06/2015 10:33:34	31.11	4	30.89	1	0.22
F101_02	07/06/2015 11:10:25	30.85	3	30.58	1	0.28
F203	07/06/2015 18:42:36	30.41	3	30.30	1	0.11
F202	07/06/2015 22:01:53	29.96	4	29.78	1	0.18
F301_01	07/07/2015 08:05:57	29.45	5	28.97	1	0.47
F301_02	07/07/2015 08:16:34	29.59	5	29.05	1	0.55
F301_03	07/07/2015 08:42:57	29.71	5	28.97	1	0.74
F302	07/07/2015 09:43:17	29.49	7	28.35	1	1.14
F303	07/07/2015 10:44:58	29.00	7	28.48	1	0.52
F404_01	07/07/2015 17:48:11	29.62	6	29.10	1	0.52
F404_02	07/07/2015 18:35:25	29.43	6	28.81	1	0.62
A01_01	07/10/2015 14:23:28	29.16	5	28.89	3	0.27
A01_02	07/10/2015 14:35:21	29.22	5	28.88	3	0.33
A01_03	07/10/2015 14:56:49	29.16	5	28.91	3	0.24
A01_04	07/10/2015 15:27:26	29.09	4	28.83	1	0.26
2A01	07/13/2015 16:46:01	29.99	5	29.52	2	0.47
2A12	07/14/2015 15:12:41	26.98	8	26.63	6	0.34
2A13	07/14/2015 15:58:16	27.33	9	26.78	5	0.54
2F501_02	07/15/2015 08:36:15	26.76	9	26.47	6	0.29
2F405	07/16/2015 11:47:20	29.44	10	29.19	5	0.25

Note: A station number beginning with 2 means that the station was visited during the second leg of the cruise. For example, F101_01 is Sta. F101, cast 1, whereas 2F501_02 is Sta. F501, cast 2, but for the second leg.

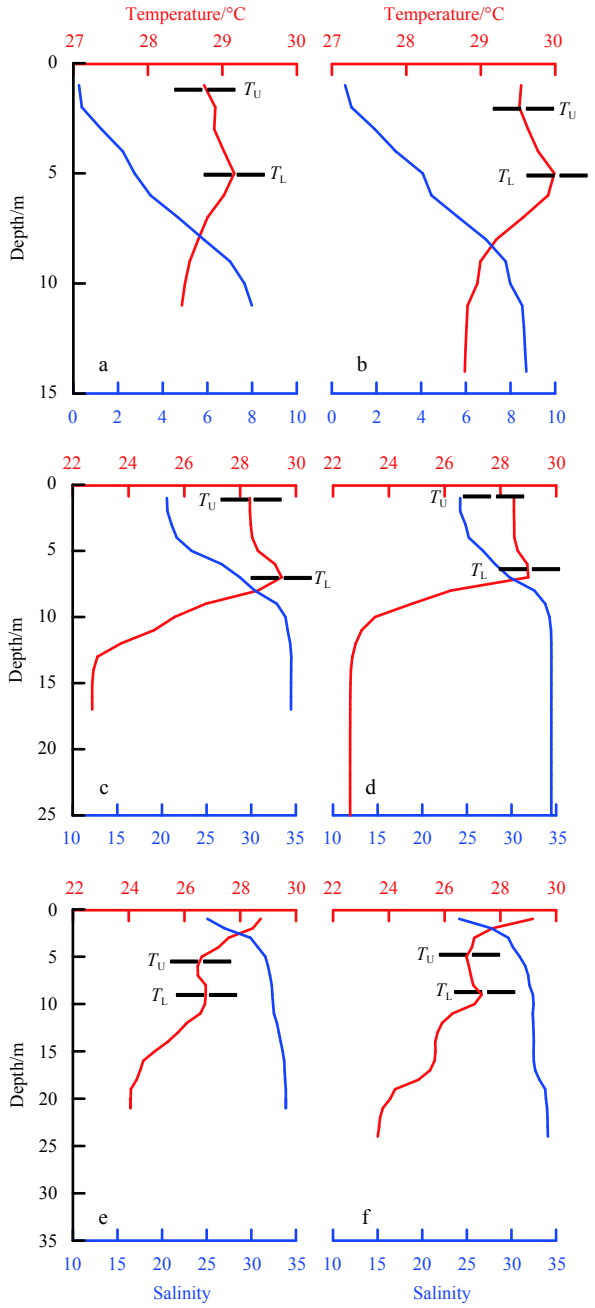

Fig. 5. Vertical distributions of temperature and salinity at Stas A01 (a), 2A01 (b), F302_01 (c), F303 (d), 2F501 (e), and 2A13 (f).

Stas A01 and 2A01. Before the measurement was conducted at Sta. A01 on July 10, Typhoon Linfa had passed the ZRE at night on July 9, causing cooling in the majority of the ZRE. The observational data from the fixed-point buoy station indicate a very low daily averaged air temperature and SST on July 10. After the typhoon disappeared, the overall water temperature rose by 1°C at 2A01 on July 13, and the inversion phenomenon became more pronounced. However, no inversion layer was observed at other stations near A01. This indicates that the cooling induced by the typhoon was not the major reason for the inversion. As shown in Figs 1 and 2, Sta. A01 is located at the confluence of the Shiziyang Channel, Jiaomen Channel and Taiping Waterway in the estuary. Figures 6a and b show the distributions of temperature and salinity at Section P06-A01-A03 and the distributions of currents par-

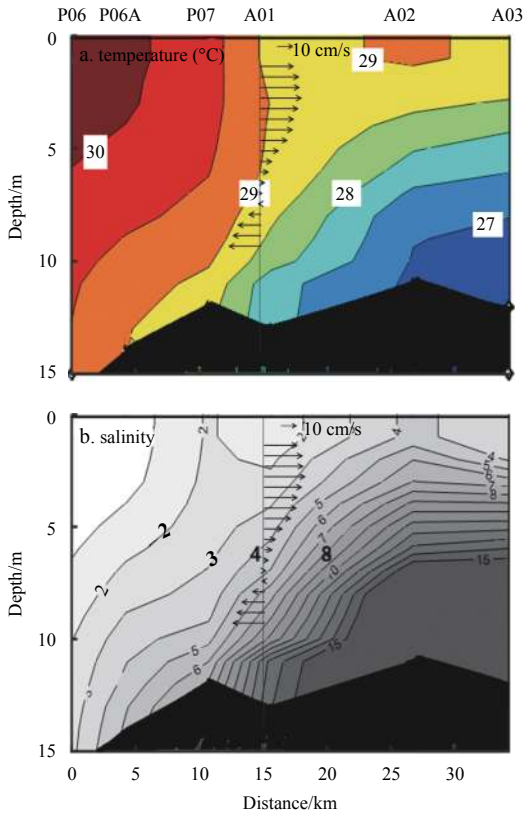

Fig. 6. Distributions of temperature (a), salinity (b) and velocity (vectors in a and b) for Section P06-A01-A03 during the cruise.

allel to the cross-section at Sta. A01 during the observation period. The recorded water temperature at Sta. P07 (upstream) was about 1.5°C greater than that at A02 (downstream). The current vectors at each layer parallel to the cross-section in Sta. A01 were consistent with the temperature and salinity contours. In the inversion layer, the maximum velocity was from P07 to A01, thus forming the temperature reversal phenomenon at Sta. A01. At Sta. 2A01, observed on the second leg of cruise, not only the temperature and salinity distributions (mentioned above) but also the current patterns were approximately the same as at A01. It can therefore be inferred that the temperature inversion layer observed at Sta. A01 formed through the same dynamic mechanism during both legs of the cruise.

In Zone 2, the similarity in the characteristics of the detected inversion layer at all seven stations again indicates that it was created by the same mechanism at each location. As shown in Fig. 2 and Fig. 7c, stations with an inversion layer in this zone are mainly located in the salinity front of the estuary. The difference in surface water temperature between the two water masses is greater than 2°C, which is one of the conditions for forming such an inversion phenomenon. Because of the presence of salinity fronts in estuaries, the distribution of isopycnals resembles the distribution of isohalines. Therefore, when two water masses encounter each other, the relatively low-salinity and low-density water will overlap the relatively high-salinity and high-density water, forming a stable inversion layer. Section F3 is taken as an example, as follows.

The cruise data show inversion phenomena at Stas F301, F302 and F303 of Section F3 (Fig. 1). As shown in Fig. 8a, the temperature at F302, located on the relatively low salinity side of the sec-

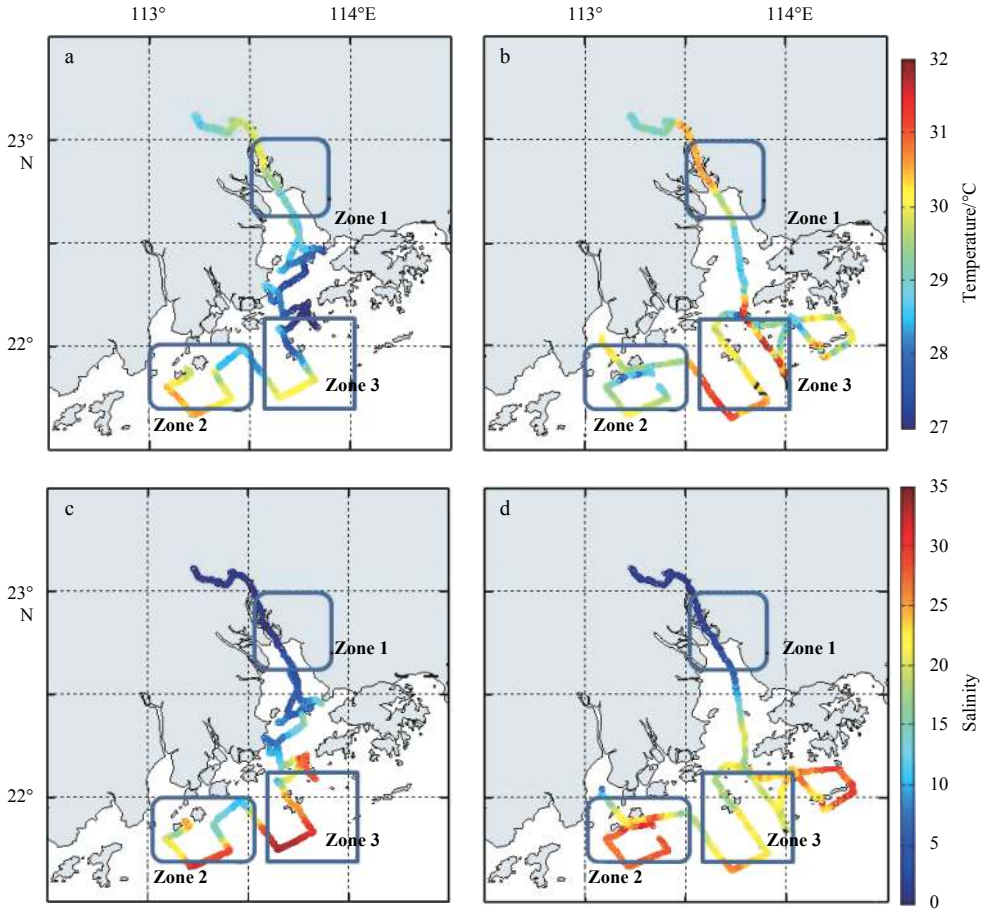

Fig. 7. Distributions of salinity and temperature at the sea surface based on measurements of the shipborne thermosalinograph during the cruise. a. Temperature during the first leg; b. temperature during the second leg; c. salinity during the first leg; and d. salinity during the second leg.

tion, is 28.3°C, and the temperature at F305, on the relatively high salinity side of the section, is 30.1°C. In general, the observation data show that the surface temperature on the low salinity side is about 2°C lower than that on the high salinity side (Figs 8b and c). The data are most consistent with the inversion layer forming when relatively low-temperature, low-salinity and low-density water mass encounters the relatively high-temperature, high-salinity and high-density water mass at the front and the former overlaps the latter. After the passage of the typhoon, the SST in the ZRE rose rapidly during the second leg of the cruise, which was consistently reflected by the data from the fixed-point station (Fig. 3) and the shipborne thermosalinograph. Figure 7b shows that during the second leg, the SST difference between the two sides of the salinity front was smaller. For example, though there was also a salinity front in Section 2F3 that was similar to Section F3 from the first leg of the cruise, the SST difference between 2F305 (30.8°C at 1 m depth) and 2F302 (30.5°C at 1 m depth) was only 0.3°C and did not lead to the occurrence of an inversion in this zone at that time.

Due to the typhoon, it was not possible to make complete observations in Zone 3 in the first leg, so only observation data from the second leg were used to characterize and analyze the temperature inversion. The results in Figs 2, 7b and 7d show that the stations showing inversion phenomena are mainly located in the salinity front off southwestern Hong Kong. These observations were made between July 14 and 15. The temperature and salinity observations show that there was a low-temperature and high-salinity center near southwestern Hong Kong and that in Zone 3, specifically, the difference in surface temperature between the two sides of the salinity front was less than 0.5°C. Thus, inversion such as that seen at Zone 2 was not observed in the upper surface of the frontal region. As shown in Fig. 9, the isohalines in Section 2A show a significant uplift at Sta. 2A13 with an impact depth of 5–10 m, which is consistent with the upper and lower boundaries of the inversion phenomenon observed in the second leg. In the 5 m layer, there is a significant low-temperature and high-salinity center at 2A13 compared to stations to either side. As also shown in Figs 7b and d, a significant low-temperature and high-salinity center was observed (22.2°N, 114.0°E) in the north of Zone 3, i.e., south of Hong Kong. The low-temperature and high-salinity water then intruded in the 5 m layer, accounting for the presence of the inversion layer in the intermediate layer.

5 Conclusions

Temperature inversion phenomena were observed in the ZRE in the summer of 2015 using cruise measurements. The main conclusions of the present study are summarized as follows.

(1) Temperature inversion was observed primarily in three zones. Zone 1 was at the confluence of the Shiziyang Channel, the Taiping Channel and the Jiaomen Channel, Zone 2 was in the west of the ZRE, and Zone 3 was off southwestern Hong Kong. The results show that the temperature difference in the inversion

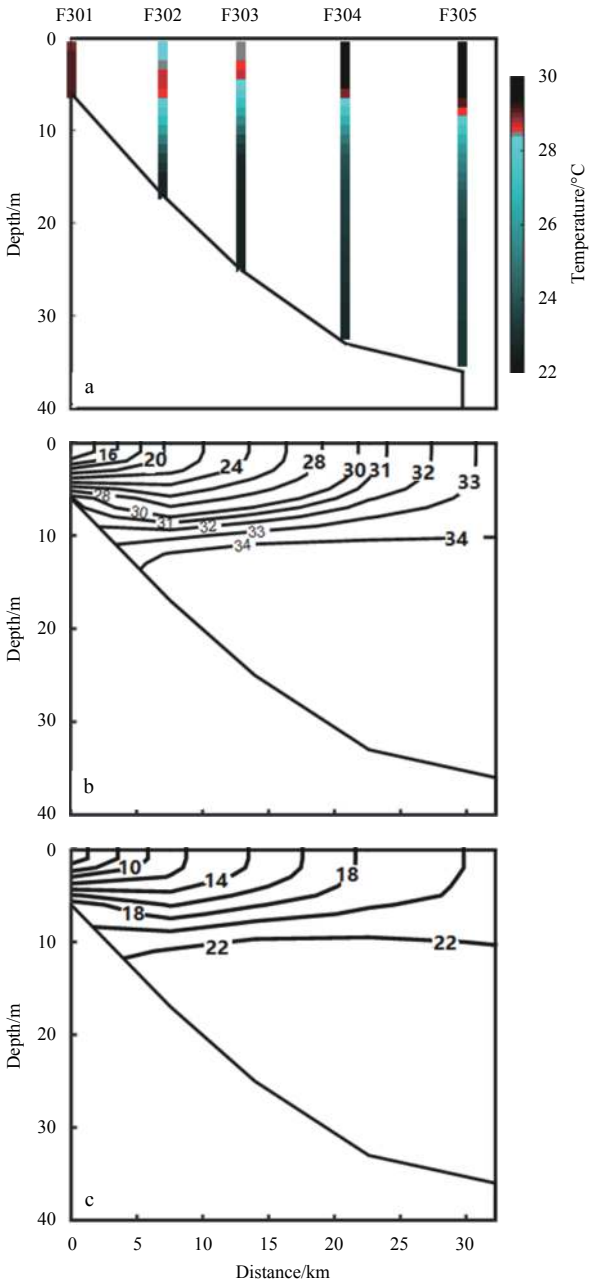

Fig. 8. Distributions of temperature (°C) (a), salinity (b) and potential density (kg/m^3) (c) for Section F3 during the cruise.

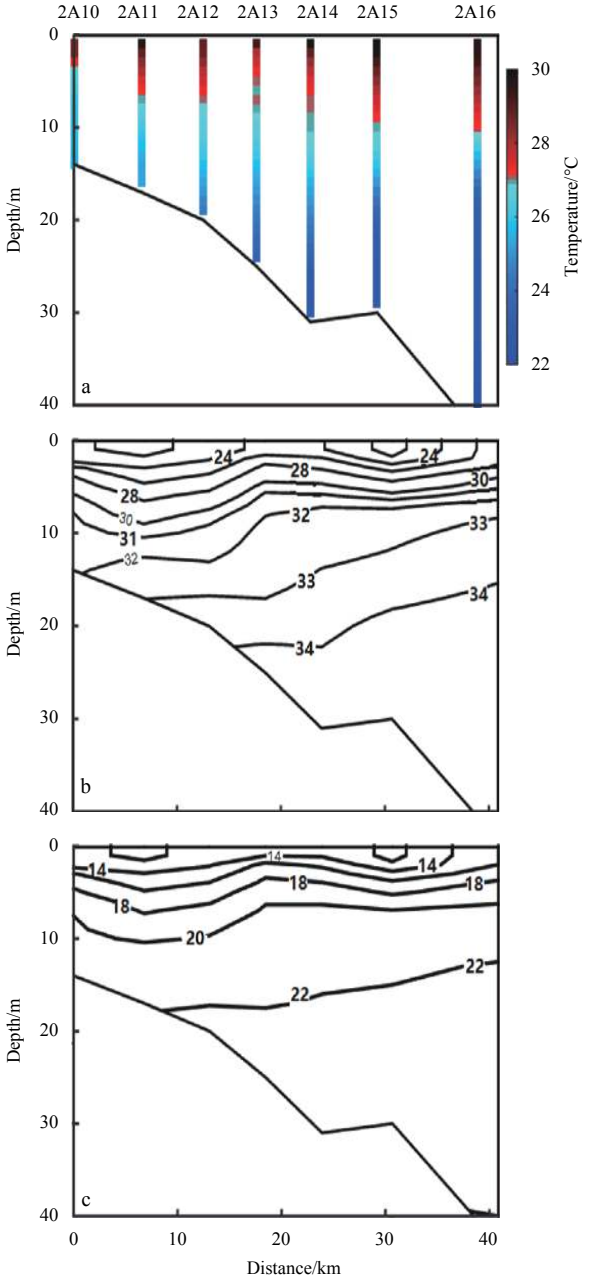

Fig. 9. Distributions of temperature (°C) (a), salinity (b) and potential density (kg/m^3) (c) for Section 2A during the cruise.

layer is 1.14°C at Stas F302 and F302, near the center of the salinity front. In Zones 1 and 2, the upper bound of the inversion layer was at the surface and the lower boundary was at a depth of 3–7 m. In Zone 3, the upper boundary was at a depth of approximately 5 m and the lower boundary was at 8–10 m. The average thickness of the inversion layer was about 4 m. Observations show that different dynamic mechanisms are responsible for the formation of temperature inversion in the three zones.

(2) Zone 1 lies at the confluence of three channels. An inversion phenomenon was observed at Sta. A01 and also at Sta. 2A01 three days later. There was a difference of about 1.5°C in the water temperature between adjacent Stas P07 and A02 on either side of Sta. A01, and current flow was in a direction parallel to the line connecting P07 and A02 at A01. The maximum flow velocity was parallel to Section P06-A01-A03, resulting in the intrusion of warm water from upstream and thus forming the inversion layer in this area.

(3) Zone 2 is located at the estuarine salinity front on the west side of the ZRE. During the first leg of the cruise, the surface water temperature in the fresh frontal area was relatively low due to the typhoon. In Section F3, the SST difference was about 2°C. Thus, it is concluded that in Zone 2, the temperature reversal was caused by the density difference because relatively low-temperature, low-salinity water overlapped relatively high-temperature, high-salinity water. During the second leg of the cruise, the temperature difference on either side of the salinity front decreased (less than 0.5°C), resulting in the disappearance of the inversion phenomenon in this zone.

(4) Zone 3 is mainly located to the southwest of Hong Kong.

Affected by the low temperature and high salinity of the water on the south side of Hong Kong, relatively low-temperature water was formed below the mixed layer of diluted water near the front, resulting in a reversal of the temperature below it.

Acknowledgements

We thank the crew of R/V *Kediao No. 8* and all participants in the cruise for their efforts in field work.

References

Akhil V P, Durand F, Lengaigne M, et al. 2014. A modeling study of the processes of surface salinity seasonal cycle in the Bay of Bengal. Journal of Geophysical Research: Oceans, 119(6): 3926–3947, doi: 10.1002/2013JC009632

Chen Xianyao, Qiao Fangli, Ge Renfeng, et al. 2006. Development of subsurface warm water in the East China Sea in fall. Journal of Geophysical Research: Oceans, 111(C11): C11S10

Dong Lixian, Su Jilan, Wong L A, et al. 2004. Seasonal variation and dynamics of the Pearl River plume. Continental Shelf Research, 24(16): 1761–1777, doi: 10.1016/j.csr.2004.06.006

Girishkumar M S, Ravichandran M, McPhaden M J. 2013. Temperature inversions and their influence on the mixed layer heat budget during the winters of 2006–2007 and 2007–2008 in the Bay of Bengal. Journal of Geophysical Research: Oceans, 118(5): 2426–2437, doi: 10.1002/jgrc.20192

Han Weiqing, McCreary J P Jr, Kohler K E. 2001. Influence of precipitation minus evaporation and Bay of Bengal rivers on dynamics, thermodynamics, and mixed layer physics in the upper Indian Ocean. Journal of Geophysical Research: Oceans, 106(C4): 6895–6916, doi: 10.1029/2000JC000403

Hou Weifen, Yu Cungen, Zheng Ji, et al. 2010. The distribution characteristics of temperature in the offshore waters of Southern Zhejiang Province. Journal of Zhejiang Ocean University (Natural Science) (in Chinese), 29(1): 59–63

Lan Shufang, Gu Chuancheng, Fu Bingzhao. 1993. Inversion phenomenon of temperature and salinity in the continental shelf region of East China Sea. Transactions of Oceanology and Limnology (in Chinese), 3: 28–34

Mao Qingwen, Shi Ping, Yin Kedong, et al. 2004. Tides and tidal currents in the Pearl River Estuary. Continental Shelf Research, 24(16): 1797–1808, doi: 10.1016/j.csr.2004.06.008

Nagata Y. 1967. Shallow temperature inversions at ocean station V. Journal of the Oceanographical Society of Japan, 23(4): 194–200, doi: 10.5928/kaiyou1942.23.194

Nagura M, Terao T, Hashizume M. 2015. The role of temperature inversions in the generation of seasonal and interannual SST variability in the far northern Bay of Bengal. Journal of Climate, 28(9): 3671–3693, doi: 10.1175/JCLI-D-14-00553.1

Nisha K, Rao S A, Gopalakrishna V V, et al. 2009. Reduced near-surface thermal inversions in 2005–06 in the southeastern Arabian Sea (Lakshadweep Sea). Journal of Physical Oceanography, 39(5): 1184–1199, doi: 10.1175/2008JPO3879.1

Ou Suying, Zhang Hong, Wang Dongxiao, et al. 2007. Horizontal characteristics of buoyant plume off the Pearl River Estuary during summer. Journal of Coastal Research, 50: 652–657

Qiu Yun, Xu Jindian, Guo Xiaogang, et al. 2012. Temperature inversion in the Taiwan Strait during Northeast monsoon. Haiyang Xuebao (in Chinese), 34(2): 13–22

Thadathil P, Gopalakrishna V V, Muraleedharan P M, et al. 2002. Surface layer temperature inversion in the Bay of Bengal. Deep Sea Research Part I: Oceanographic Research Papers, 49(10): 1801–1818, doi: 10.1016/S0967-0637(02)00044-4

Thadathil P, Gosh A K. 1992. Surface layer temperature inversion in the Arabian Sea during winter. Journal of Oceanography, 48(3): 293–304, doi: 10.1007/BF02233989

Ueno H, Yasuda I. 2005. Temperature inversions in the subarctic North Pacific. Journal of Physical Oceanography, 35(12): 2444–2456, doi: 10.1175/JPO2829.1

Wong L A, Chen J C, Xue H, et al. 2003a. A model study of the circulation in the Pearl River Estuary (PRE) and its adjacent coastal waters: 1. Simulations and comparison with observations. Journal of Geophysical Research: Oceans, 108(C5): 3156

Wong L A, Chen J C, Xue H, et al. 2003b. A model study of the circulation in the Pearl River Estuary (PRE) and its adjacent coastal waters: 2. Sensitivity experiments. Journal of Geophysical Research: Oceans, 108(C5): 3157, doi: 10.1029/2002JC001452

Yan Wenbing. 1991. The inversion thermocline in Taiwan Strait. Journal of Oceanography in Taiwan Strait (in Chinese), 10(4): 334–337

Yuan Dongliang, Li Yao, He Lei, et al. 2010. An observation of the three-dimensional structure of a cross-shelf penetrating front off the Changjiang mouth. Deep Sea Research Part II: Topical Studies in Oceanography, 57(19–20): 1827–1834, doi: 10.1016/j.dsr2.2010.04.009

Zu Tingting, Gan Jianping. 2015. A numerical study of coupled estuary–shelf circulation around the Pearl River Estuary during summer: Responses to variable winds, tides and river discharge. Deep Sea Research Part II: Topical Studies in Oceanography, 117: 53–64, doi: 10.1016/j.dsr2.2013.12.010

Zu Tingting, Wang Dongxiao, Gan Jianping, et al. 2014. On the role of wind and tide in generating variability of Pearl River plume during summer in a coupled wide estuary and shelf system. Journal of Marine System, 136: 65–79, doi: 10.1016/j.jmarsys.2014.03.005